Tunable photonic band gap in self-assembled clusters of floating magnetic particles

Y. Saado,[1] M. Golosovsky,[1,*] D. Davidov,[1] and A. Frenkel[2]
[1]*The Racah Institute of Physics, The Hebrew University of Jerusalem, 91904 Jerusalem, Israel*
[2]*ANAFA—Electromagnetic Solutions Ltd. P.O.B. 5301, Kiriat Bialik 27000, Israel*
(Received 22 March 2002; revised manuscript received 30 July 2002; published 22 November 2002)

We fabricated a 3D photonic crystal consisting of metal coated disk-shaped magnetic particles floating at the liquid-air interface inside a stack of containers. The particles self-assemble into an ordered crystal whose in-plane lattice constant can be varied by external magnetic field in very broad limits. This crystal exhibits photonic stopband at microwave frequencies. The stopband can be continuously tuned by external magnetic field until complete disappearance.

DOI: 10.1103/PhysRevB.66.195108 PACS number(s): 42.70.Qs, 81.16.Dn

I. INTRODUCTION

Photonic crystals are two-dimensional (2D) or three-dimensional (3D) ordered structures composed of millimeter to nano-sized objects. When these structures are periodic, their refractive index is spatially modulated. Therefore, they exhibit strong ''Bragg'' reflections[1] associated with the opening of a band-gap in the photonic Brillouin zone. Today there is a quest for tunable photonic bandgap materials, since tunability allows external modulation, or at least fine-tuning of the crystal parameters at the fabrication process. Several directions to achieve tunability have been explored theoretically and few of them have been realized experimentally. In particular, tunability in semiconductor structures may be achieved by varying temperature[2] (through its effect on the plasmon frequency) or by varying voltage[3] (in the structures with $p-i-n$ transitions). Tunability can be also achieved by liquid crystal infiltration in inverse opal structure,[4–6] application of elastic stress,[7] or by using magnetic field.[8–12] In the last case the tunability is achieved via Faraday effect in one of the constituents or via field dependence of the magnetic permeability. Most of these ways result in few percent variation of the lattice constant, yet the extreme sensitivity of the photonic bandgap in dielectric mixtures to the symmetry and crystal parameters allows considerable variation in the bandgap.

We use self-assembly under magnetic forces[11–22] and explore the possibility of achieving tunability in self-assembled photonic crystals via variation of the in-plane lattice constant. Magnetic field dependence of the lattice constant in such systems has been reported recently[11,12,19–21] and its usefulness for photonic crystals in the optical range has been demonstrated.[11,12] We report here 3D metal-dielectric photonic crystals with a magnetically tunable in-plane lattice constant. The tunability is so high that the bandgap may completely disappear.

While our photonic crystals are too big to be useful in their present form, they represent a nice model system to explore tunability of the in-plane lattice constant and its effect on photonic bandgap. Having in view applications in the infrared and optical range, it is possible to reduce the size of the crystal by going to colloidal magnetic particles. In this context, the most promising applications will be (*i*) the control of the self-assembly of the three-dimensional photonic crystals at the fabrication stage and (*ii*) the control of surface plasmon propagation along the conducting layer immersed in a two-dimensional tunable photonic crystal based on colloidal magnetic particles in the liquid.

II. EXPERIMENTAL SETUP

Figure 1(a) shows a 2D-structure self-assembled from composite particles consisting of a Styrofoam disk covered with a conducting coating, and a small cylindrical axially-magnetized NdFeB permanent magnet attached to the center

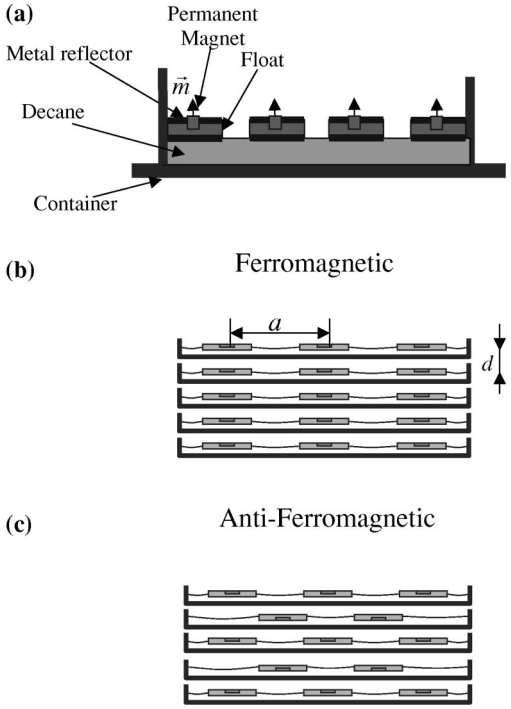

FIG. 1. Particle arrangement. (a) 2D particle configuration in a container. The particle size is $D_f=30$ mm, $h_f=2$ mm. The size of the NdFeB magnet is $D_m=5$ mm, $h_m=2$ mm. Container wall thickness is 2 mm and the thickness of the liquid layer is 6 mm. Air-gap between the layers is 12 mm. (b) ''Ferromagnetic'' configuration (direction of the magnetic moment is the same in all layers). (c) ''Antiferromagnetic'' configuration (direction of the magnetic moment alternates between successive layers).

of the disk. These composite particles float on the liquid-air interface in a transparent plexiglass container. In the equilibrium state the particles self-assemble into hexagonally-ordered cluster due to magnetic repulsion. The liquid serves two goals: (*i*) lubrication—to allow self-assembly driven by weak lateral forces and (*ii*) stabilization against the flip. A side-effect introduced by the liquid—weak capillary attraction between the particles—is negligible compared to magnetic repulsion. In the absence of an external magnetic field the particle configuration depends on container shape and on particle number. For certain ''magic'' particle numbers ($Z=37$, $Z=61$, etc.) and for hexagonally-shaped container the defect-free configuration is achieved.[19] The in-plane lattice constant a is determined by the particle number Z and by the external magnetic field.

Several containers are mounted in a stack [Figs. 1(b) and 1(c)]. The separation between containers is small enough to allow magnetic interaction across the stack. There are two possible configurations: ''ferromagnetic'' [Fig. 1(b)] and ''antiferromagnetic'' [Fig. 1(c)]. For the ''ferromagnetic'' configuration the direction of the particle magnetic moment is the same in all containers. If we consider only nearest neighbors, the in-plane particle interaction is repulsive, while the out-of-plane interaction is attractive. Consequently, the particles arrange in columns stretching across the stack. For ''antiferromagnetic'' configuration the direction of the particle magnetic moment alternates between successive layers. Here, the in-plane and out-of-plane nearest-neighbor interactions are repulsive, hence the particles acquire a chess-like configuration.

The ''ferromagnetic'' configuration allows us to tune the in-plane lattice constant by external magnetic field (Fig. 2). We perform such tuning by a current-carrying coil (500 turns, $R=20$ cm and $h=10$ cm) encircling the stack. The coil produces an axial magnetic field with a radial gradient which, for $r\sim 0.9R$, can approximated by:

$$B(r)\approx B_0\left(1+0.75\frac{r^2}{R^2-r^2}\right), \tag{1}$$

where B_0 is the field in the center of the coil. When the field is antiparallel to the particle magnetic moment, the particles are pushed towards the center of container, while in the opposite case they are pushed towards the periphery. To tune the lattice constant we use the antiparallel field configuration.

The container stack and the coil are mounted inside a 60×60 cm^2 chamber covered by the microwave absorber (Fig. 2). We choose decane ($C_{10}H_{22}$) as a lubricating liquid due to its low refraction index and low microwave losses. Transmission measurements were performed using an HP-8510C vector network analyzer and two wide-band (2–18 GHz) antennae separated by 80 cm. To prevent multiple reflection paths which do not pass through the sample, we mounted above it an absorbing screen with a 30 cm diameter aperture. Each particle configuration has been photographed by a CCD camera. The crystal symmetry and the in-plane lattice constant were determined using MATLAB image processing toolbox. We studied microwave transmission in the range 2–10 GHz,

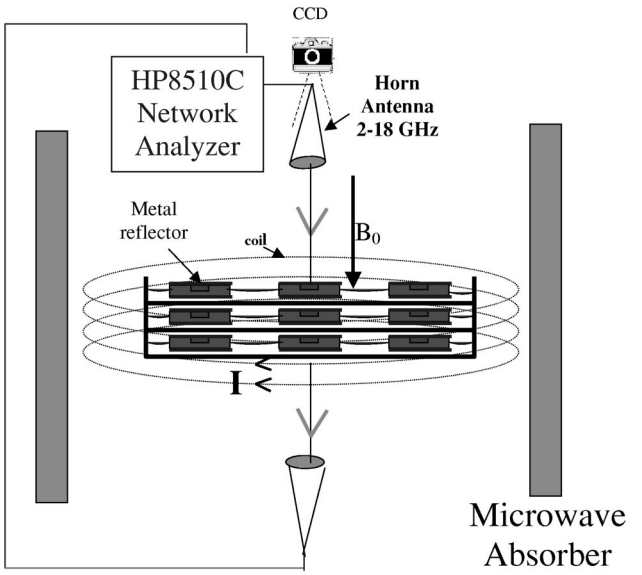

FIG. 2. Experimental setup. The stack with containers is mounted inside the current-carrying coil which produces magnetic field with radial gradient. The whole fixture is mounted inside a chamber with the sides covered by a microwave absorber. Microwave transmission measurements have been performed using two 2–18 GHz antenna separated by 80 cm.

at normal incidence, as a function of the interlayer distance, number of layers, and the in-plane lattice constant.

III. PARTICLE ARRANGEMENT IN EXTERNAL MAGNETIC FIELD

Figure 3 shows that identically-oriented particles self-assemble into a 3D hexagonally-ordered column array which may be compressed by external magnetic field. It is noteworthy that the internal symmetry of the array remains unchanged upon magnetic field variation. The lattice constant is quite uniform across the crystal. A detailed analysis shows, however, that there is a small radial gradient, although the average elastic deformation does not exceed 4%–5% for $Z\sim 100$ particles.

To determine the particle configuration we write down the Hamiltonian which reduces here to potential energy:

$$H=E_{\rm int}+E_{\rm field}=\frac{\mu_0}{4\pi}\sum_{i<j}\frac{M_iM_j}{|r_i-r_j|}+\sum_{i=1}^{N}M_iB(r_i)l. \tag{2}$$

We make a very rough assumption that the crystal consists of long axially-magnetized columns of length l with magnetization per unit length M. The first term in Eq. (2) is the interaction energy between the columns and the second term is the energy in the external field. We substitute Eq. (1) into Eq. (2), introduce distance and energy scales

$$r_0=\left(\frac{\mu_0MR^2}{3\pi B_0l}\right)^{1/3};E_0=\frac{\mu_0M^2}{4\pi r_0}, \tag{3}$$

and recast Eq. (2) in dimensionless form:

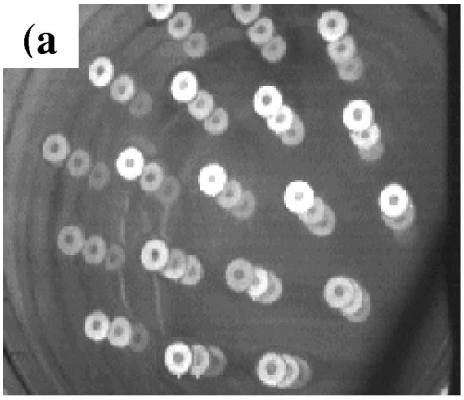

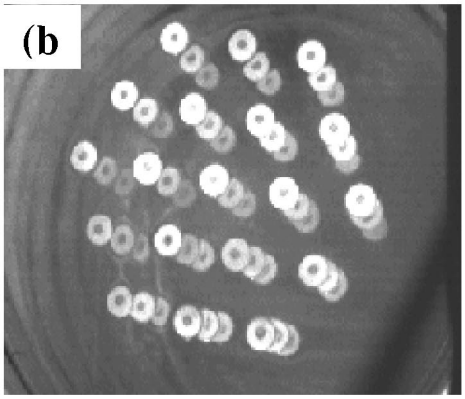

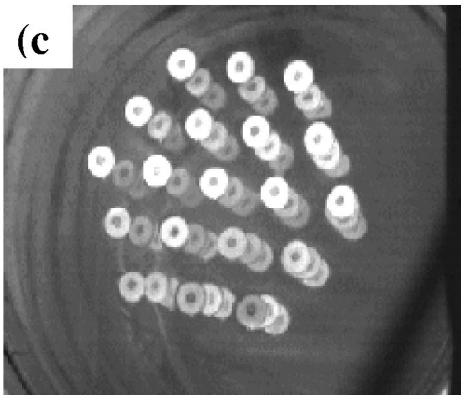

FIG. 3. A photonic crystal (three layers, ferromagnetic configuration, $Z=37$ particles in each layer). Magnetic field in the center of the array increases from 0.4 mT in (a) to 1.2 mT in (c). Note corresponding lattice constant decrease.

$$E=E_{\text{int}}+E_{\text{field}}=\sum_{i<j}\frac{1}{|r_i-r_j|}+\sum_{i=1}^{N}\frac{r_i^2}{1-r_i^2/R^2}. \qquad (4)$$

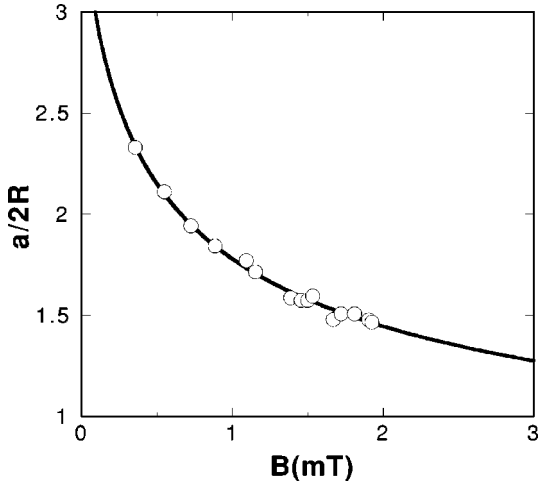

FIG. 4. The in-plane lattice constant a as a function of magnetic field for a five-layer photonic structure (''ferromagnetic'' configuration). The solid curve shows model approximation, $a\sim B_0^{-1/3}$ where B_0 is the field in the center of the coil. R is the particle radius.

Equation (3) suggests the power-law dependence of the in-plane lattice constant $a\sim r_0\sim B_0^{-1/3}$ which agrees well with our experimental results (Fig. 4). Note that the lattice constant can be reversibly changed by 50%. Too strong compression is precluded by the loss of stability due to particle flip.

IV. COMPUTER SIMULATIONS

We used ANSOFT-HFSS 3D Maxwell Equation solver to calculate microwave transmission and reflection through the periodic structure shown in Fig. 1. The solver is based on the finite element method (FEM) and has the option to analyze a single unit cell out of infinite periodic array by employing periodic boundary conditions. Exploiting this capability we modeled the exact geometry of a lateral unit cell that includes the container stack, the liquid, and the floating magnets covered with conducting foil. Proper material properties were assigned to each component, including dielectric losses. Periodic boundary conditions for normal incidence were assigned, and higher propagating Floquet modes were taken into account whenever the lattice constant exceeded one wavelength. The solver divides the geometrical model into a large number of simple polygons (tetrahedrals) and adaptively refines the mesh to reach convergent results for transmission coefficients. After completing the adaptive solution at upper frequency, a fast frequency sweep, based on advanced Pade approximation, was used to recover the solution over a wide band of frequencies. The main simplifying approximation here was the use of the square rather than hexagonal lattice of scatterers for each layer, due to some limitations of the solver. We kept the filling factor of the square lattice identical to that of the hexagonal lattice measured in the experiments. Calculations with finite hexagonal lattices in HFSSS and a complementary comparison with the Finite Difference Time Domain (FDTD) solver CST Microwave

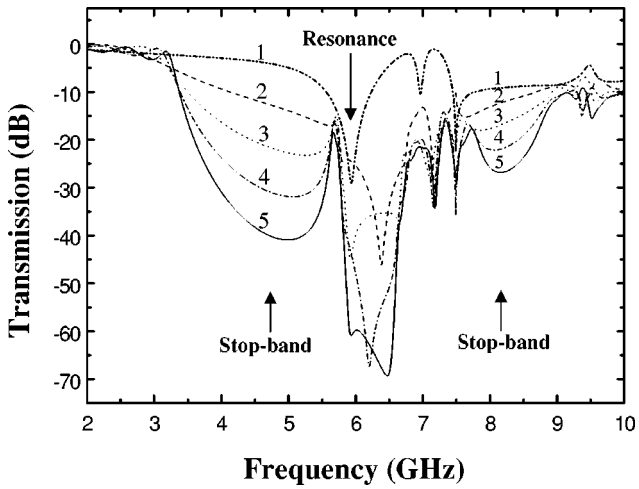

FIG. 5. Computer simulation of the microwave transmission through photonic structure (''ferromagnetic'' configuration). The number of layers is shown at each curve. Note almost full transmission at low frequencies and the stopband at 3.2–5.7 GHz.

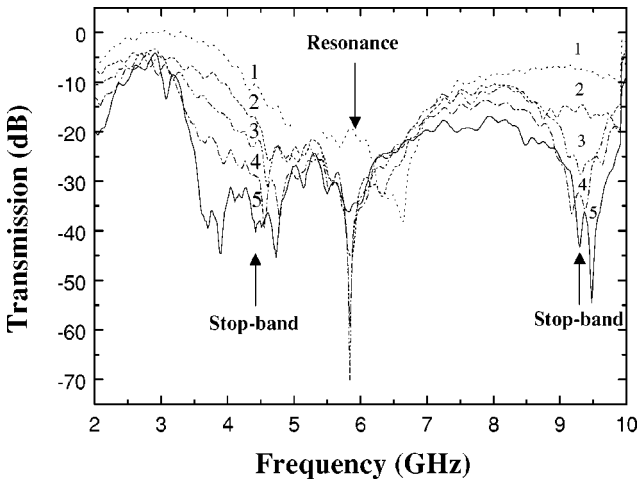

FIG. 6. Experimentally measured microwave transmission through photonic structure. The number of layers is shown at each curve. Note the stopband at 3–5.1 GHz.

Studio[23] showed that at least for normal incidence the results are very similar to those of the square lattice.

We used the simulations to identify the photonic bandgap and to optimize the structure for the widest stopband. We varied the disk size, the separation between the layers and the in-plane lattice constant. Finally, we chose the optimal combination of parameters for which the 3–6 GHz stopband was most pronounced and fabricated the experimental structure accordingly. At the next step we simulated all the variations of the structure that has been tested experimentally: different number of layers, lattice constant and arrangement.

V. MICROWAVE TRANSMISSION THROUGH PHOTONIC CRYSTAL

The microwave transmission through the stack of containers containing only liquid is rather high and exhibits a dip at ~6 GHz (not shown here). This dip corresponds to Bragg reflection from the layered dielectric structure. When we insert the particles, the transmission spectrum is more complicated and depends now on the particle concentration (filling factor).

Figure 5 shows computer simulation of the microwave transmission at normal incidence as a function of number of layers for the ''ferromagnetic'' configuration [Fig. 1(b)]. We observe several regions. Below 3.2 GHz there is almost complete transparency and the microwave transmission hardly changes upon increase in layer number. Between 3.2 and 5.7 GHz a photonic stopband develops. Transmission becomes progressively smaller upon increasing number of layers, each layer introduces ~10 dB attenuation. Between 6 and 6.2.7 GHz there appears a sharp dip, probably a resonance, whose frequency slightly varies depending on whether the number of layers is even or odd. This dip is followed by the region of relative transparency. Above 7.7 GHz another, less pronounced stopband appears.

Figure 6 shows corresponding experimental results. The overall agreement between simulations (Fig. 5) and experimental results is quite satisfactory. Indeed, below 3.2 GHz the microwave transmission is rather high and is nearly independent of the number of layers. The dip at 2 GHz is probably related to cut-off effect in antennae. Between 3.2 and 5 GHz there is a clear photonic stopband. Between 5 and 7 GHz there is a broad dip followed by the region of relative transparency where transmission is almost independent on the number of layers. Around 9 GHz there develops another stopband.

''Ferromagnetic'' configuration offers the unique possibility to vary the lattice constant by external magnetic field. Figure 7 shows computer simulation of the microwave transmission at normal incidence for a five-layer crystal. Upon increasing in-plane lattice constant the stopband shrinks in such a way that the low-frequency edge remains almost constant while the high-frequency edge moves to lower frequencies. The depth of the stopband hardly changes until, for some lattice constant a, the gap abruptly disappears leaving behind a small dip. The sharp dip at 5.9–6.4 GHz also disappears.

Figure 8 shows corresponding experimental results. The overall agreement between simulations (Fig. 7) and experimental results is quite satisfactory. Upon increasing lattice constant the stopband shrinks and eventually disappears. The low-frequency edge hardly changes while the high-frequency edge moves to low frequencies.

VI. DISCUSSION AND CONCLUSIONS

The metal-dielectric structures are exceptional among photonic crystals in that their stopband is wide[24] and robust. Indeed, it is determined by the filling factor and by the local symmetry while the long-range order plays a minor role.[25] Our computer simulations also do not show high sensitivity to in-plane symmetry and even suggest similar transmission spectra for ''ferromagnetic'' and ''antiferromagnetic'' configurations [Figs. 1(b) and 1(c)].

The basic understanding of the transmission spectra in our

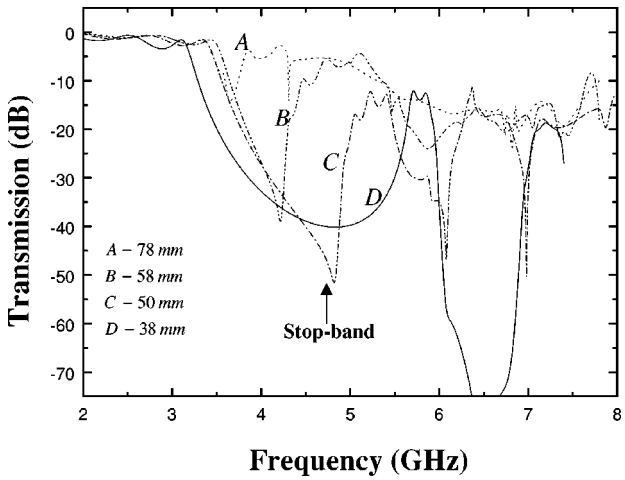

FIG. 7. Computer simulation of the microwave transmission through a five-layer photonic structure for different values of the in-plane lattice constant *a*. Note shrinking and eventual disappearance of the stopband upon increasing lattice constant.

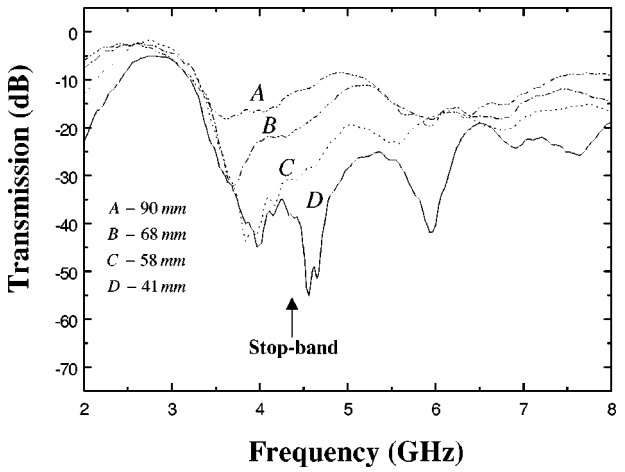

FIG. 8. Experimentally measured microwave transmission through photonic structure for the different values of the in-plane lattice constant. Note shrinking and eventual disappearance of the stopband upon increasing lattice constant.

samples is achieved by considering (*i*) transmittance of the Bragg reflector,[26] and (*ii*) Mie resonance of conducting disks.[27] Indeed, our sample may be represented by a Bragg reflector with the unit cell shown in Fig. 1(a). Since refractive indices of the liquid ($n=1.45$) and of the plexiglass ($n=1.65$) are rather close, we consider our unit cell as a two-layer structure, where one layer is the air gap ($d_1=12$ mm, $n_1=1$) and another layer is an effective medium consisting of the dielectric ($d_2=8$ mm, $n_2=1.5$) with embedded conducting disks. In the absence of the disks this structure represents a quarter-wavelength Bragg reflector, since $n_1d_1 \approx n_2d_2$. Upon insertion of conducting disks the effective refraction index of the liquid layer increases and depends now on the filling ratio, ordering, and (frequency-dependent) polarizability of a single disk.

Transmittance of the Bragg reflector at normal incidence is[26]

$$T=\frac{t_1}{t_1+r_1\sin^2(NKd)/\sin^2(Kd)}, \tag{5}$$

where t_1 and r_1 are transmission and reflection coefficients of the single layer, N is the number of layers, K is the wavevector, and d is the interlayer spacing.

Bragg reflector exhibits its first gap at $Kd=\pi$ that corresponds to

$$f_0=\frac{u_p}{2(n_1d_1+n_2d_2)}, \tag{6}$$

where u_p is the phase velocity. The gap width is

$$\Delta f/f_0 \approx \frac{4}{\pi}\frac{n_2-n_1}{n_2+n_1}. \tag{7}$$

The imaginary part of the wavevector at the center of the gap is

$$\mathrm{Im}(Kd)=2\frac{n_2-n_1}{n_2+n_1}. \tag{8}$$

Then Eq. (5) yields exponentially small transmittance in the gap

$$T=\frac{t_1}{t_1+r_1\sinh^2[N\mathrm{Im}(Kd)]/\sinh^2[\mathrm{Im}(Kd)]}$$

$$\sim\frac{t_1}{r_1}e^{-2(N-1)\mathrm{Im}(Kd)}. \tag{9}$$

For the five-layer sample and in the absence of conducting disks our measurements yield the gap centered at $f_0=5.8$ GHz, with the width of $\Delta f/f_0 \sim 0.4$ and attenuation in the gap of ~ 2.4 dB/layer (not shown here). This satisfactorily agrees with the estimates based on Eqs. (6)–(9), namely, $f_0=6$ GHz, $\Delta f/f_0=0.25$, and attenuation of 2.8 dB/layer. Upon insertion of conducting disks the central frequency of the gap moves down, $f_0=4.5$ GHz, the width increases $\Delta f/f_0=0.4-0.55$, and the attenuation increases up to 8–9 dB/layer (Figs. 5 and 6). Using Eqs. (6)–(9) for this new configuration we deduce that upon insertion of conducting disks the effective refraction index of the liquid layer changes from $n_2=1.5$ to $n_2^{\mathrm{eff}}=2.67$. This yields $f_0=4.5$ GHz, $\Delta f/f_0=0.58$ and attenuation of 8 dB/layer which is in good agreement with above experimental/computational results.

Consider now the effect of the disks on the overall frequency dependence of the mm-wave transmission. According to Eqs. (5) and (9), the whole transmission spectra can be roughly represented as a single layer transmittivity t_1 multiplied by a Bragg factor ($\sin^2 NKd/\sin^2 Kd$). At low frequencies the conducting disks do not play a major role since their size is much smaller than the wavelength (Rayleigh limit). However, upon increasing frequency the scattering crossection of the disks increases and achieves a maximum at first Mie resonance ($KR=1.6$[27]). We relate the dip in transmission at 6.2 GHz (Figs. 5 and 6, transmission through one

layer) to the Mie resonance of conducting disk. This frequency differs from that expected for a single disk (5.1 GHz in air) due to the coupling between adjacent disks and the in-plane ordering.

To account for the dependence of the transmittivity on the in-plane ordering and lattice constant (Figs. 7 and 8) we adopt a different approach which is analogous to the tight-binding approximation[28] (while the complementary approach based on effective medium[29] is analogous to the model of nearly free electrons in solid-state physics). Following Ref. 25 we relate the high-frequency edge of the photonic stopband in the metal-dielectric structures to the cut-off effect in the voids between conducting particles. Indeed, assume closely packed conducting disks. The voids between them represent waveguides (this is especially evident for column-like particle arrangement). Short waves can freely squeeze in the voids between the columns. The high-frequency edge of the photonic stopband corresponds to the cut-off in the void given by

$$f_{hf}=\frac{u_p}{2d_{\text{void}}} \tag{10}$$

where u_p is the phase velocity and d_{void} is the size of the void. For closely packed hexagonal lattice of conducting disks $d_{\text{void}}\sim(\sqrt{3}-1)R$ where R is the disk radius. Upon increasing lattice constant the size of the voids increases and adjacent voids become coupled. When the lattice constant is big enough, the coupling is so strong that the cut-off effect disappears. Both these factors yield inverse dependence of the high-frequency edge of the stopband on the lattice constant (Figs. 7 and 8). Note also that, upon increasing lattice constant, the notion of the voids starts to lose sense, hence the dip in transmission does not have steep edges anymore (Figs. 7 and 8). This reminds us of the results of Ref. 30 that reports the less steep stopband in the metal-dielectric photonic crystals upon increasing disorder. The resulting dip in transmission is better represented as Mie resonance of individual uncoupled scatterers[31] rather than as a stopband.

Our findings may be compared to recent results of Serpenguzel[32] who studied photonic bandgap in the fcc lattice of metallic spheres in the microwave range. Serpenguzel observes a wide stopband in the microwave range with approximately the same depth as ours. The central frequency and the width of the stopband in Ref. 32 are approximately four times higher, as expected from inverse scaling with the particle size. However, since the Mie resonances in conducting sphere and in conducting disk are strongly different, we observe Mie resonance (Figs. 5– 8) in addition to the stopband, while Ref. 32 observes only the stopband.

In conclusion, we demonstrate a five-layer photonic crystal exhibiting stopband in the microwave range at normal incidence. We modulate the in-plane lattice constant by external magnetic field and achieve 100% tunability of the stopband. The magnetic field dependence of the photonic stopband parameters is qualitatively understood. The tunability considerably exceeds that previously achieved in superparamegnetic colloidal crystals.[11] Although our particles are quite macroscopic, the scaling down is achievable and quite recently we succeeded to go to smaller particles and to achieve tunable stopband also in the mm-wave range.

ACKNOWLEDGMENTS

This work was supported by the VW foundation, the Israeli Ministry of Science and Arts, and by the Israeli Science Foundation. We are grateful to Y. Neve-Oz for his help in the experiment and computer simulations.

*Electronic mail: golos@vms.huji.ac.il

[1] J. D. Joannopoulus, R. D. Meade, and J. N. Winn, *Photonic Crystals Molding the Flow of Light* (Princeton University Press, Princeton, NJ, 1995).
[2] P. Halevi and F. Ramos-Mendieta, Phys. Rev. Lett. **85**, 1875 (2000).
[3] A. de Lustrac, F. Gadot, S. Cabaret, J.M. Lourtioz, T. Brillat, A. Priou, and E. Akmansoy, Appl. Phys. Lett. **75**, 1625 (1999).
[4] K. Busch and S. John, Phys. Rev. E **58**, 3896 (1998).
[5] D. Kang, J.E. Maclennan, N.A. Clark, A.A. Zakhidov, and R.H. Baughman, Phys. Rev. Lett. **86**, 4052 (2001).
[6] C.S. Kee, H. Lim, Y.K. Ha, J.E. Kim, and H.Y. Park, Phys. Rev. B **64**, 085114 (2001).
[7] S. Kim and V. Gopalan, Appl. Phys. Lett. **78**, 3015 (2001).
[8] D. Lacoste, F. Donatini, S. Neveu, J.A. Serughetti, and B.A. Van Tiggelen, Phys. Rev. E **62**, 3934 (2000).
[9] B. Gates and Y.N. Xia, Adv. Mater. **13**, 1605 (2001).
[10] A. Figotin, Y.A. Godin, and I. Vitebsky, Phys. Rev. B **57**, 2841 (1998).
[11] X.L. Xu, G. Friedman, K.D. Humfeld, S.A. Majetich, and S.A. Asher, Adv. Mater. **13**, 1681 (2001).
[12] E.L. Bizdoaca, M. Spasova, M. Farle, M. Hilgendorf, and F. Caruso, J. Magn. Magn. Mater. **240**, 44 (2002).
[13] K. Zahn, R. Lenke, and G. Maret, Phys. Rev. Lett. **82**, 2721 (1999).
[14] R. Bubeck, C. Bechinger, S. Neser, and P. Leiderer, Phys. Rev. Lett. **82**, 3364 (1999).
[15] R. Seshadri and R.M. Westervelt, Phys. Rev. B **46**, 5142 (1992).
[16] I.V. Schweigert, V.A. Schweigert, and F.M. Peeters, Phys. Rev. Lett. **84**, 4381 (2000).
[17] A.S. Dimitrov, T. Takahashi, K. Furusawa, and K. Nagayama, J. Phys. Chem. **100**, 3163 (1996); T. Takahashi, A.S. Dimitrov, and K. Nagayama, *ibid.* **100**, 3157 (1996).
[18] R.E. Kusner, J.A. Mann, and A.J. Dahm, Phys. Rev. B **51**, 5746 (1995).
[19] M. Golosovsky, Y. Saado, D. Davidov, Appl. Phys. Lett. **75**, 4168 (1999); Y. Saado, M. Golosovsky, D. Davidov, and A. Frenkel, Synth. Met. **116**, 427 (2001).
[20] B.A. Grzybowski, H.A. Stone, and G.W. Whitesides, Nature (London) **405**, 1033 (2000).
[21] W.J. Wen, L.Y. Zhang, and P. Sheng, Phys. Rev. Lett. **85**, 5464 (2000).
[22] H. Loewen, J. Phys.: Condens. Matter **13**, R145 (2001).
[23] CST GmbH, Budinger Str. 2a 64289, Darmstadt, Germany.
[24] S. Fan, P.R. Villeneuve, and J.D. Joannopoulos, Phys. Rev. B **54**, 11 245 (1996).

[25] W.Y. Zhang, X.Y. Lei, Z.L. Wang, D.G. Zheng, W.Y. Tam, C.T. Chan, and P. Sheng, Phys. Rev. Lett. **84**, 2853 (2000).
[26] A. Yariv and P. Yeh, *Optical Waves in Crystals* (Wiley, New York, 1984), Ch. 6.
[27] H. C. Van de Hulst, *Light Scattering by Small Particles* (Wiley, New York, 1957), p. 337.
[28] E. Lidorikis, M. M Sigalas, E.N. Economou, and C.M. Soukoulis, Phys. Rev. Lett. **81**, 1405 (1998).
[29] V. Yannopapas, A. Modinos, and N. Stefanou, Phys. Rev. B **60**, 5359 (1999).
[30] M. Bayindir, E. Cubukcu, I. Bulu, T. Tut, E. Ozbay, and C.M. Soukoulis, Phys. Rev. B **64**, 195113 (2001).
[31] M.M. Sigalas, C.T. Chan, K.M. Ho, and C.M. Soukoulis, Phys. Rev. B **52**, 11 744 (1995).
[32] A. Serpenguzel, IEEE Microwave Wireless Components Lett. **12**, 134 (2002).